

CSMCNet: Scalable Video Compressive Sensing Reconstruction with Interpretable Motion Estimation

Bowen Huang, Xiao Yan, Jinjia Zhou, and Yibo Fan

Abstract—Most deep network methods for compressive sensing reconstruction suffer from the black-box characteristic of DNN. In this paper, a deep neural network with interpretable motion estimation named CSMCNet is proposed. The network is able to realize high-quality reconstruction of video compressive sensing by unfolding the iterative steps of optimization based algorithms. A DNN based, multi-hypothesis motion estimation module is designed to improve the reconstruction quality, and a residual module is employed to further narrow down the gap between reconstruction results and original signal in our proposed method. Besides, we propose an interpolation module with corresponding training strategy to realize scalable CS reconstruction, which is capable of using the same model to decode various compression ratios. Experiments show that a PSNR of 29.34dB can be achieved at 2% CS ratio (compressed by 98%), which is superior than other state-of-the-art methods. Moreover, the interpolation module is proved to be effective, with significant cost saving and acceptable performance losses.

Index Terms—Compressive sensing, motion estimation, deep unfolding, interpolation, scalable reconstruction.

I. INTRODUCTION

COMPRESSIVE sensing, firstly introduced by Candes, Tao and Donoho in 2006 [1], is a novel sampling technique. This method enables exact reconstruction of original signal from much fewer samples compared with classic Nyquist sampling rule requires. Though traditional compression methods, such as JPEG and H.264, still have a wide range of application, CS has the special characteristic of sensing and compression simultaneously. This property will lead to brand new encoder and decoder systems, which has potential value in specific areas, such as single pixel camera [2], magnetic resonance imaging(MRI) equipment [3], and high-speed video system [4].

The sampling process of CS can be described as $y = \Phi x$, where $x \in R^N$ is the original signal, $\Phi \in R^{M \times N}$ is the measurement matrix, and $y \in R^M$ consists of the samples. The compression ratio can be defined as $CR = \frac{M}{N}$. In CS, fast measurement can be achieved by sampling part of x with

This work was supported by Japan Science and Technology agency (JST) PRESTO Grant Number JPMJPR1757 Japan. This work was supported in part by the National Natural Science Foundation of China under Grant 62031009, in part by the Shanghai Science and Technology Committee (STCSM) under Grant 19511104300, in part by Alibaba Innovative Research (AIR) Program, in part by the Innovation Program of Shanghai Municipal Education Commission, in part by the Fudan University-CIOMP Joint Fund(FC2019-001). (Corresponding author: Yibo Fan.)

Bowen Huang, Xiao Yan and Yibo Fan are with the State Key Laboratory of ASIC and System, Fudan University, Shanghai 200433, China (e-mail: bw Huang19@fudan.edu.cn; 19112020084@fudan.edu.cn; fanyibo@fudan.edu.cn).

Jinjia Zhou is with the Graduate School of Science and Engineering, Hosei University, Tokyo 184-8584, Japan (e-mail: jinjia.zhou.35@hosei.ac.jp).

$M \ll N$.

Theoretically, to get exact reconstruction, x should have some structure-inducing regularizers [5], for example, the original signal should be sparse in some transformation domains [6], [7], which means it can be formulated as $s = \Psi x$, where Ψ is called sparsity basis or sparsity matrix, and s is the sparse representation of x . Though it is difficult for natural images and videos to achieve true sparsity in one specific transformation domain, CS allows approximate sparsity as well, at the cost of recovery with losses.

With measurement matrix Φ and sparsity matrix Ψ , we can modify the encoding process of CS into $y = \Phi \Psi^{-1} s$. According to CS theory, Φ and Ψ should obey restricted isometry property, or RIP rule [8], [9]. Fortunately, RIP rule has been proved to be equivalent to sampling matrix and sparsity matrix being mutually incoherent [10], and random matrix is commonly chosen since it meets the requirement in most cases. Additionally, some other matrix is also used. For instance, random binary matrix is specially designed for hardware realization, and 2D-DCT matrix has more concentrated energy in the DC component [11]. Recently, some research is done on structured random matrix(SRM), where part of random elements are replaced by manually designed structure. Experiments show that SRM can provide additional benefits, such as preserving neighbour information or reducing computation and memory consumption [12], [13].

The CS reconstruction is to solve an under-determined linear inverse problem. Recovery methods are developed by using prior assumptions about images, such as sparsity, to narrow the solution space. The corresponding optimization model of CS reconstruction can be described as follows

$$\min_x \phi(x) \quad s.t. \quad y = \Phi x \quad (1)$$

where $\phi(x)$ is the regularization term.

Instead of reconstruct x directly, we usually solve s at first, and then get x by $x = \Psi^{-1} s$. The constrained standard reconstruction model of s is

$$\hat{s} = \arg \min_x \frac{1}{2} \|\Phi \Psi s - y\|_2^2 + \lambda \|s\|_1 \quad (2)$$

where \hat{s} is the reconstruction result. Based on this model, various optimization algorithms have been exploited [6], [14]–[18]. Besides, driven by the powerful learning capabilities of neural networks, a number of DNN-based approaches have been applied [4], [19]–[22]. Classical DNN methods use deep network to map the input compressive measurements to the output reconstruction results directly. Stacked by convolution layers and activate functions, deep neural network can learn

non-linear mapping from large training dataset efficiently. Moreover, algorithm unrolling [23] is developed based on optimization methods and DNN structure. According to this technique, each iteration is mapped into a stage of the network, and multiple stages form a cascaded structure, offering promise in developing interpretable network. Several networks have applied this technique on CS reconstruction, such as ADMM [3] and ISTA [24], and all achieve good experimental results in reconstruction quality and computation speed.

Another area of concern is that all aforementioned recovery methods are general for image and video compressive sensing, but there is additional information embedded in video sequences. Image CS reconstruction methods cannot utilize inter-frame reference of video sequences, which is widely used in traditional video compression methods. The motion estimation is important to improve reconstruction quality and our preliminary work in [25] proposed a method that attempts to use adjacent frames to improve the reconstruction performance of video CS. To the best of our knowledge, it is the first work that utilize algorithm unrolling to develop explicit motion estimation structure in DNN for video CS reconstruction.

In this work, we further extend our preliminary work by adding an interpolation module, named ITP module. This new network, dubbed CSMCNet-ITP, enables scalable reconstruction under conditions of different CS ratios with only one model. Compared with the existing deep learning based methods, CSMCNet-ITP helps saving storage in mobile devices and embedded systems, and reducing training cost. Furthermore, experimental results prove that the proposed ITP module can be added to existed reconstruction networks with only a little change, and the original recovery performance doesn't descend much. This feature adds to the versatility of our proposed method.

In summary, the main contributions of this paper are as follows:

- 1) We use neural network modules to replace the optimization steps in the conventional model-based approaches and unfold it into hierarchical architecture that supports end-to-end training.
- 2) We propose a multi-hypothesis motion estimation module realized by fully-connected layers. The module generates motion estimation from reference window in the adjacent frame and helps improving the final reconstruction results.
- 3) An interpolation module is proposed to solve scalable sampling and reconstruction with only one model, saving memory and improving flexibility at the cost of little performance degradation. The interpolation module can be plugged into other existed deep networks, helping them to complete scalable CS tasks.

The paper is organized as follows. Section II introduces the background of block-based CS and multi-hypothesis motion estimation, and list some related works. Section III and IV describe the details of CSMCNet and CSMCNet-ITP. Section V shows the experimental results. In Section VI, we conclude this paper.

II. BACKGROUND

A. Block-based Compressive Sensing

To alleviating the huge computation and memory burdens when the input image has high resolution, block-based compressive sensing(BCS) is introduced in [26]. According to BCS, one can break the image into smaller blocks and process each block independently. Suppose that an image is divided into $B \times B$ non-overlapping blocks, and x_i is a vector representing block i of input image X in raster-scan fashion. The aforementioned encoding equation is modified as:

$$y_i = \Phi_B x_i \quad (3)$$

where Φ_B is a $M_B \times B^2$ measurement matrix and the compression rate is $CR = \frac{M_B}{B^2}$. It is straightforward to see that BCS in (3) is equivalent to apply a whole-image measurement matrix Φ with a diagonal constraint

$$\Phi = \begin{bmatrix} \Phi_B & 0 & \cdots & 0 \\ 0 & \Phi_B & \cdots & 0 \\ \vdots & & \ddots & \vdots \\ 0 & \cdots & 0 & \Phi_B \end{bmatrix} \quad (4)$$

To coordinate with the blocked measurement matrix, the sparsity matrix Ψ should also be a block-based operator of the same $B \times B$ size.

In this paper, the block size of 16 is used, which achieves balance of computation burdens and reconstruction performance in our method. However, BCS will produce blocking artifacts in general, and additional deblocking operations must be applied to eliminate it. Some methods [18], [27], [28] use independent deblocking module, such as BM3D, and some DNN methods [29], [30] also perform image reconstruction and deblocking at the same time. We choose BM3D as a post-process denoiser in this article.

B. Multi-hypothesis Motion Estimation

In traditional video compression methods, motion estimation(ME) and motion compensation(MC) is long employed to improve performance in H.264, H.265, etc. In consideration of bit rate limitation, these algorithms use single hypothesis MEMC in order to reduce the amount of motion vectors. However, this limitation doesn't exist in CS, since MEMC is executed at the decoder side of the system. Therefore, multi-hypothesis MEMC is considered to get better prediction results.

A multi-hypothesis prediction can be described as an optimal linear combination of all possible reference blocks in the search window of the reference frame

$$\omega_{t,i} = \arg \min_{\omega} \|x_{t,i} - \tilde{x}_{t,i}(\omega)\|_2^2 \quad (5)$$

$$\tilde{x}_{t,i}(\omega) = \omega_{t,i} H_{t,i} \quad (6)$$

where the subscript t is the index of frame in the video and i is the index of image block in the frame. The $H_{t,i}$ is a matrix of dimensionality $K \times B^2$, consisted of rasterizations of the K possible reference blocks. In this context, $\omega_{t,i}$ is the coefficient that represents the linear combination of the possible reference

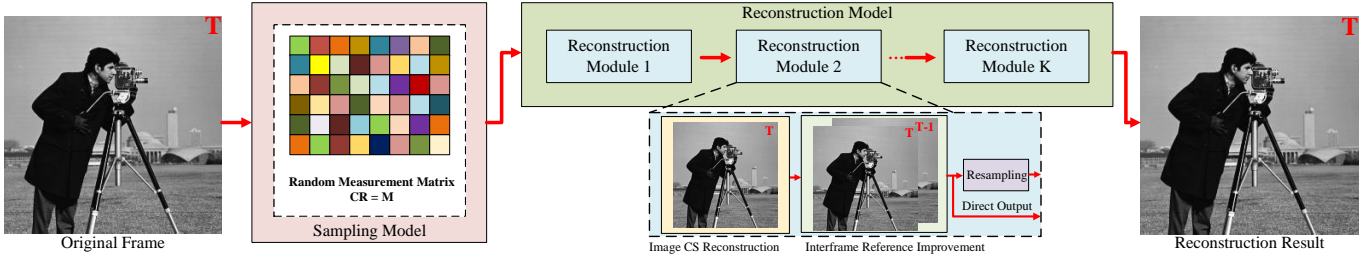


Fig. 1. The sampling and reconstruction process of CSMCNet. Every reconstruction module includes image CS reconstruction and inter-frame reference improvement. Several reconstruction modules are stacked to simulate the iteration steps.

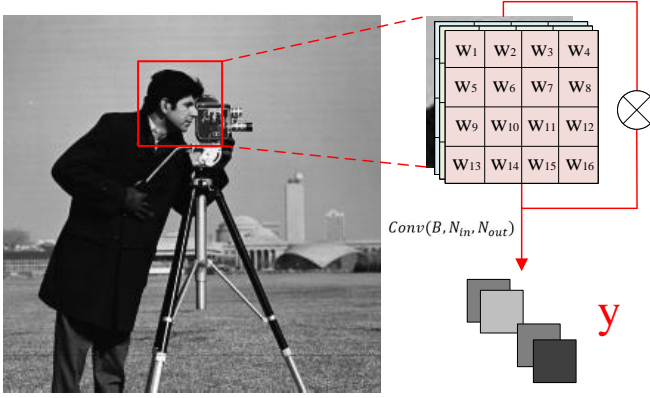


Fig. 2. The measurement process of CSMCNet based on BCS. CS measurements are sampled through convolution.

blocks.

In the case of CS reconstruction, (5) cannot be implemented directly, since $x_{t,i}$ is unknown, and only measurements $y_{t,i}$ is accessible. To solve this dilemma, (5) can be modified as

$$\hat{\omega}_{t,i} = \arg \min_{\omega} \|y_{t,i} - \Phi \omega_{t,i} H_{t,i}\| \quad (7)$$

where $\hat{\omega}_{t,i} \neq \omega_{t,i}$ generally. One commonly chosen solution to this ill-posed problem in conventional algorithms is Tikhonov regularization [15], while in this paper we propose a learning-based module to solve it, which appears better prediction ability.

Besides, some other network structure, such as RNN, is also used to extract temporal information in video CS reconstruction [20]. With the help of algorithm unrolling, we are able to design more explicit structure to implement MEMC, and experiments show that our methods achieve superior performance due to the targeted optimization compared with the RNN based methods.

C. Related Works

Roughly speaking, there are three kinds of recovery algorithms that have been developed, i.e. optimization-based iterative algorithms, end-to-end DNN methods and hybrid reconstruction methods.

For optimization-based reconstruction methods, the general idea is to find efficient regularization terms inspired by image priors. Sparsity in some transformation domains, such as DCT [31], wavelet [17] and gradient domain [14], has been

exploited to rebuild image and video signal. For instance, Li *et al.* [14] used the total variation(TV) regularizer for improving the local smoothness. Metzler *et al.* [32] combined the BM3D denoiser with the AMP algorithm, dubbed D-AMP, to achieve better reconstruction quality. For video CS, Fowler *et al.* [15] proposed a motion compensation and block-based method with projected Landweber reconstruction algorithm, in which additional reference information was obtained to help recovery. Yang *et al.* [33] used Gaussian mixture model(GMM) to recover high-frame-rate video measurements, and the reconstruction could be computed from the probabilistic model updated online. The advantage of these methods is that they usually have theoretical guarantee. However, due to the nature of iteration, the computation time of these methods is relatively long, which makes them unsuitable for real-time application. Moreover, their performance largely relies on the hand-designed prior constraints, which are difficult to decide.

For classic end-to-end data-driven deep neural networks, Mousavi *et al.* [27] is the first one that apply stacked denoising auto-encoder to solve CS reconstruction problem. Lohit *et al.* [28] proposed a CNN consisted of fully connected layers and convolution layers, and a BM3D denoiser was used for de-blocking in postprocessing. There are also some deep networks developed for video CS specifically. Xu *et al.* [20] proposed a network named CSVideoNet, in which a multi-rate CNN and a synthesized RNN was combined to improve the trade-off between compression rate and spatial-temporal resolution of the reconstructed videos. Iliadis *et al.* [4] designed a deep fully-connected network for video compressive sensing, and the measurement matrix was trained with the recovery network coherently to improve the final results.

Compared with iterative methods, these networks benefits from their feed-forward architecture, making inference of results very fast. Additionally, parameters learned through training achieve better performance. Nevertheless, suffering from the black box characteristic of these models, there is no good interpretation and theoretical guarantee for these methods, bringing difficulty in making targeted improvements. Thus, it will be beneficial to integrate the ideas of conventional algorithms and deep neural networks.

For scalable CS, some networks aiming at multi-rate CS competent for the task. Shi *et al.* [30] proposed a scalable CNN called SCSNet. The network was composed of several sub-networks, each of which solved one specific compression rate to provide coarse granular scalability. A greedy algorithm

was used to accomplish finer granular scalability. Xu *et al.* [34] proposed a scalable Laplacian pyramid reconstructive adversarial network(LAPRAN) that enabled flexible and fast CS images reconstruction. It used a hierarchical structure of multiple stages, and each stage could generate an output of different resolution at different compression rate. However, the network structure of multi-rate CS is more complex than classic ones, leading to larger model size comparably.

Apart from the above two types of methods, some research combines the prior knowledge and the structure of deep networks. Deep unfolding method unrolls iterative algorithms to integrate the advantages. For example, Zhang *et al.* [24] developed a network inspired by the Iterative Shrinkage-Thresholding Algorithm(ISTA). The network cast ISTA into deep network by solving the proximal mapping associated with the sparsity-inducing regularizer using nonlinear transforms. Wen *et al.* [35] unfolded the denoising process of approximate message passing algorithm(AMP), and an integrated deblocking module and a jointly-optimized sampling matrix were used to enhance performance. Nevertheless, no video CS reconstruction algorithm is unrolled and mapped into end-to-end network, and it is also difficult for these unfolding methods to perform adaptive reconstruction tasks due to fixed network size.

Chang *et al.* [36] proposed a general framework to train a single deep neural network that solves arbitrary linear inverse problems, including CS recovery. It was implemented through plug-and-play and the deep network acted as a quasi-projection operator of ADMM for the set of natural images. Veen *et al.* [37] used untrained deep generative models, which was based on Deep Image Prior(DIP). According to DIP, the convolution weights of the network were optimized to match the observed measurements. This method does not require pre-training over large dataset, at the cost of losing reconstruction accuracy.

III. PROPOSED CSMCNET

In this section, details of CSMCNet will be presented. As shown in Fig.1, the proposed CSMCNet is composed of an encoder(sampling model) and a decoder(reconstruction model). The sampling model is based on BCS and the reconstruction model contains several stacked stages.

Single channel video signal is mainly focused for simplicity in our paper and we declare that colorful signal can be processed channel by channel independently.

A. Sampling Model

The measurement process is implemented block-by-block as shown in Fig.2. Different from our previous work [25], where a fully connected layer was employed, we use a convolution layer to sample frames here, since convolution can be performed on input frames of arbitrary size. It can be easily proved that these are the two equivalent forms of (3). We denote this process as

$$y_{t,i} = W_s \otimes x_{t,i} \quad (8)$$

where W_s corresponds to M_B filters of kernel size $B \times B$, the subscript t is the index of frames in the video and i is

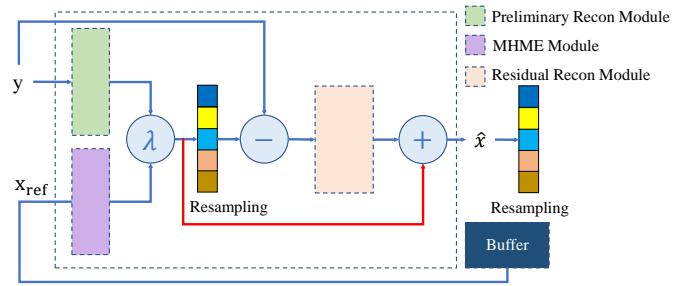


Fig. 3. The structure of the i -th reconstruction stage of CSMCNet

the index of image blocks in the frame. The stride of the convolution layer is set to be B to realize non-overlapping BCS sampling, and the compression ratio can be adjusted by change the number of filters. There is no bias and no activation function.

Research has shown that different sensing matrix, such as random Gaussian Matrix, 2D-DCT matrix and 2D-WHT matrix, has essential impact on the final results, regardless of the reconstruction algorithm [11]. An obvious reason for this influence is the fraction of the signal energy which is captured by the measurements with each sensing matrix. The 2D-DCT measurement matrix captures a much larger fraction of the signal energy, because most of the signal energy is concentrated in the low frequencies and the random matrix with normal distribution has similar effect.

It is worth noting that the first measurement, or the DC component, is similar in these matrices. Therefore, we refer only to the AC component when speaking about signal energy and measurements. In some research, jointly-trained sampling model is used to further improve recovery quality [4], [22], [28], [30], [35]. In this paper, in consideration of simplicity and flexibility, we choose random normal distribution matrix as the sampling matrix and convert it into the convolution form as described in (8).

B. Reconstruction Model

Inspired by the video CS reconstruction algorithm MC-BCS-SPL [15], the reconstruction model is established by unfolding the iterative steps. The model is composed of several hierarchical stages and each stage contains three modules, as presented in Fig.3. The reconstruction model is divided into three parts accordingly. Firstly, the preliminary reconstruction module roughly rebuilds image blocks of size $B \times B$ from input measurements $y_{t,i} \in R^M$. Secondly, multi-hypothesis motion estimation(MHME) module generates prediction from a single reference frame, which was reconstructed formerly. The MHME prediction is fused with the result of the preliminary reconstruction module as

$$\hat{x}_{t,i}^{mix} = \alpha \hat{x}_{t,i}^a + \beta \hat{x}_{t,i}^b \quad (9)$$

where $\hat{x}_{t,i}^a$ is the preliminary recovery result and $\hat{x}_{t,i}^b$ is the prediction generated from the reference frame. The coefficient α and β have the constraint of $\alpha + \beta = 1$. Empirically, we set $\alpha = \beta = 0.5$.

Thirdly, $\hat{x}_{t,i}^{mix}$ is remeasured with the same weight as in the sampling model and is subtracted from original measurements $y_{t,i}$ to get the residual measurements. The residual measurements are recovered and the final output of the stage is derived from adding the residual reconstruction results to $\hat{x}_{t,i}^{mix}$. We will introduce each module in the following paragraphs.

1) *Preliminary Reconstruction Module*: The preliminary reconstruction module contains one fully-connected layer and several convolution layers, as shown in Fig.4.

The fully-connected layer performs the same role as described in [19], and the process can be formulated as

$$\hat{x}_{t,i}(y) = W \cdot y_{t,i} + b \quad (10)$$

where $W \in R^{B^2 \times N}$ is the weight of the fully connected layer. $\hat{x}_{t,i}(y)$ is a $B \times B$ reconstructed block.

The following convolution layers all have a ReLU layer as activation function except for the last one. All feature maps have the same size as the output signal and the pooling layer is removed to preserve as much detail as possible. This process resembles the sparse coding stage in CS reconstruction, where a subset of dictionary atoms are combined to form an estimation to the original input signal.

2) *MHME Module*: As introduced in (6), the process of MHME can be represented as an linear combination of all possible reference blocks in the search window of the reference frame. Thus, it is tempting to think of using a fully connected layer to accomplish it. The weight of the linear combination is learned from large dataset and can achieve superior performance compared with optimization based solutions. Due to the similarity of adjacent frames, the aggregation of motion and spatial visual features can help improve the recovery quality compared with using image CS reconstruction methods on single frame independently.

The reference frame is the former frame that has been reconstructed. To store the reference frame, a buffer is designed as shown in Fig.3. For the sake of simplicity, we do reconstruction of current frame after the reference frame was completely reconstructed. However, the search window we use is a square with twice the size centered on the current rebuild block, and only part of the reference frame is involved. Therefore, it is possible to reduce the size of the buffer in practical application by carefully designing the reconstruction order.

3) *Residual Reconstruction Module*: To narrow down the gap between the prediction generated by MHME module and the original signal $x_{t,i}$, we use a residual reconstruction module inspired by [15], [21]. The residual reconstruction module is similar to the preliminary reconstruction module, and a skip connection is added between input and output, as shown in Fig.3. The skip connection helps to boost the network performance, and is proved useful to the convergence of deep neural network [38]. The final results can be collected to form a complete frame, as described in (11), where κ is the concatenation function that concatenates all these blocks, and h and w represent the numbers of blocks in row and column

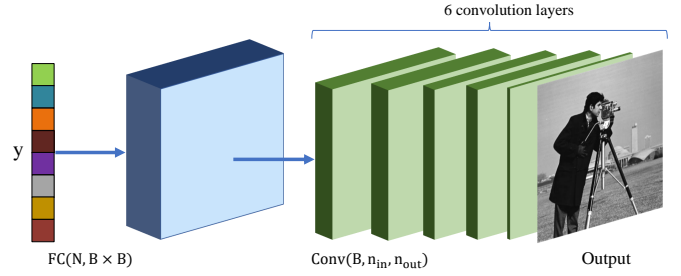


Fig. 4. The structure of the preliminary reconstruction module in CSMCNet.

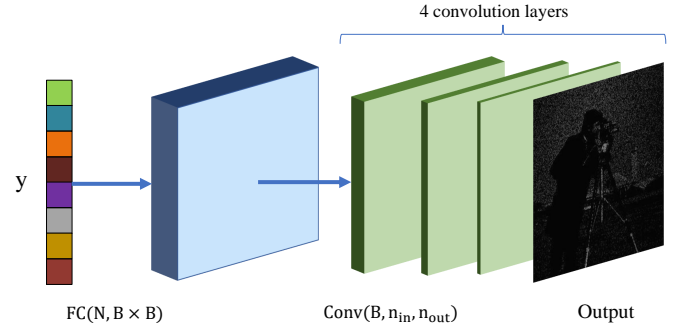


Fig. 5. The structure of the residual reconstruction module in CSMCNet.

respectively.

$$\hat{X}_t = \kappa \begin{pmatrix} \hat{x}_{t,0}(y) & \cdots & \hat{x}_{t,w-1}(y) \\ \vdots & \ddots & \vdots \\ \hat{x}_{t,(h-1)w}(y) & \cdots & \hat{x}_{t,hw-1}(y) \end{pmatrix} \quad (11)$$

IV. PROPOSED CSMCNET-ITP

The existing DNN methods cannot perform scalable sampling and reconstruction. To improve the flexibility of CSMCNet, an additional interpolation module, dubbed ITP module, is proposed in this section. In the interpolation module, an output selection strategy is employed and measurements of fixed size are produced. The produced measurements are sent to the following reconstruction model and experiments show that the ITP module has acceptable influence on the final results. Corresponding training strategy is used and we find that the ITP module can be easily plugged into existing networks.

A. ITP Module

The ITP module contains one deconvolution layer and locates before the reconstruction model in the network, as illustrated in Fig.6. Thus, the measurements obtained by the ITP module can be treated as M_B feature maps. We denote the raw measurements as $y_{t,i} \in R^{M_B \times H_C \times W_C}$, where H_C and W_C is the height and width of the feature maps. The ITP module amplifies the number of the feature maps by a factor of A , which can be regarded as a 1D deconvolution. The process can be described as follows

$$y'_{t,i} = \hat{W}^T y_{t,i} \quad (12)$$

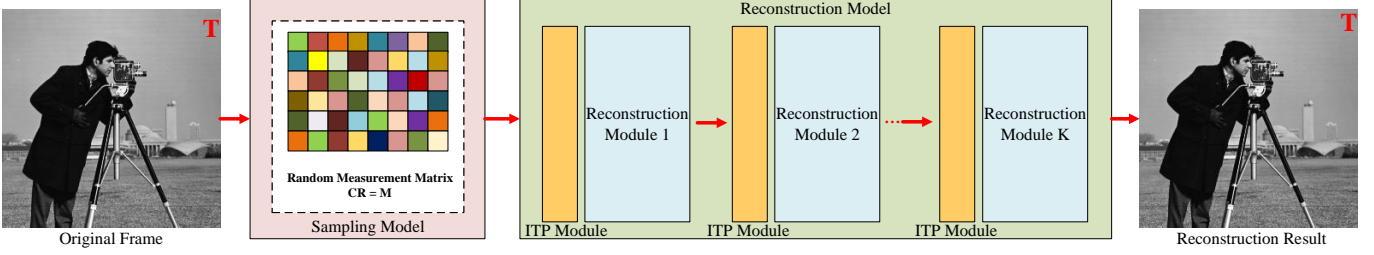


Fig. 6. The illustration of ITP module in a network with several reconstruction modules. The reconstruction modules are the same as shown in Fig.1.

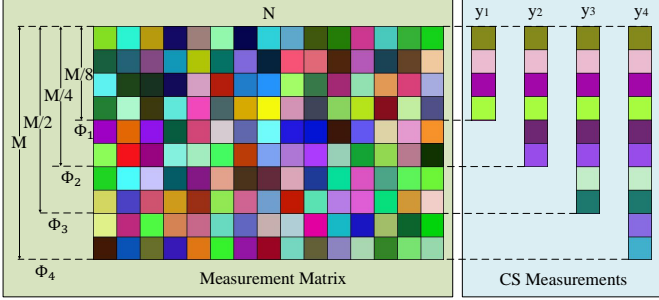


Fig. 7. The illustration of a scalable sampling process with a fixed measurement matrix. The corresponding compression ratio is 66%, 33%, 16%, 8%

where \hat{W}^T is the matrix form of the weights of convolution kernel. Suppose the transpose of the weights equals to $w_0^T, w_1^T, \dots, w_n^T$, then \hat{W}^T is

$$\hat{W}^T = \begin{pmatrix} w_0^T & 0 & 0 & \dots & 0 \\ 0 & w_1^T & 0 & \dots & 0 \\ \vdots & 0 & \dots & 0 & \vdots \\ 0 & \dots & 0 & w_{n-1}^T & 0 \\ 0 & \dots & 0 & 0 & w_n^T \end{pmatrix} \quad (13)$$

We set the amplification factor A to be $[\frac{CR_{max}}{CR_{min}}]$, with the predefined compression ratio ranges from CR_{min} to CR_{max} . For $CR_{min} \leq CR < CR_{max}$, a selection strategy is employed to choose suitable number of feature maps from the interpolation results. The strategy is designed according to the feature of 1D deconvolution and can be formulated as

$$y_{t,i}^{itp} = y'_{t,i} \lceil i \frac{CR}{CR_{min}} \rceil, \quad i = 1, 2, \dots, n \quad (14)$$

where the square bracket represents the index of $y'_{t,i}$.

Therefore, the output of ITP module has a fixed size of $M_{max} \times H_C \times W_C$, where $M_{max} = \frac{B \times B}{CR_{min}}$. These measurements with fixed size inherit the information contained in the original measurements and can be directly used in various reconstruction models. The whole process of interpolation is fast, and the detailed information on the number of module parameters and the amount of calculations is shown in Table I. We declare that this lightweight ITP module can be easily adapted to existing DNN-based reconstruction models and provides flexibility for their deployment. Experiment results are presented in Sec.V-D and Sec.V-E.

TABLE I
THE DETAILED INFORMATION OF THE PROPOSED ITP MODULE

ITEM	INFOMATION
Structure	1 1D-deconvolution layer
Input/Output Size	$L_{in} = CR \cdot B^2$ $L_{out} = CR_{max} \cdot B^2$
Parameter Number	$K = \lceil CR_{max}/CR_{min} \rceil$
MACC*	$K \times CR \times B^2$

* MACC is multiply-accumulate operations, which is commonly used as a measure of model computational complexity.

B. Training

A special training strategy is designed to improve the scalability of the network. We set the structure parameters of the reconstruction model according to the maximum compression ratio CR_{max} , and set the actual compression ratio used in the framework as a random variable, which is selected from a predefined compression ratio list. In this condition, the scalable sampling can be simply implemented by changing the number of filters of the sampling model according to the selected compression ratio, as described in Fig.7, and the ITP module will learn the interpolation coefficients efficiently.

One limitation of this training strategy is that it is not able to complete CS tasks of arbitrary compression ratio. The sampled signal can be correctly reconstructed only when the compression ratio CR used in sampling process is chosen from the predefined list of compression ratio during training. However, we argue that sufficient CR values can be added to the list during training. Five different CR value is added into the list in our experiments, and the results show that all measured signal can be rebuilt properly.

C. Loss Function

In this paper, for explicit reference, we use CSMCNet-K to represent CSMCNet with K stacked stages, and CSMCNet-ITP-K to represent K stages CSMCNet with the additional interpolation module.

The trainable parameters of CSMCNet-K contain the weight w and bias b of non-linear layers in the aforementioned three modules, and for CSMCNet-ITP-K, the parameters of the deconvolution layer in the interpolation module is also trainable. Given the training data pairs (x, x_{ref}) , we want to reduce the discrepancy between the raw signal and the reconstruction results. Additionally, we also want to enhance the prediction

TABLE II
THE DETAILED INFORMATION OF THE PROPOSED CSMCNet AND OTHER STATE-OF-THE-ART METHODS

Methods	Classification	Interpretation	flexibility	Image/Video CS	Joint training	Other characteristic
D-AMP [32]	Model based	✓	✓	Image CS		
MC-BCS-SPL [15]	Model based	✓	✓	Video CS		motion estimation
ReconNet [19]	DNN based			Image CS		
ISTANet [24]	DNN based	✓		Image CS		ISTA algorithm
AMPNet [35]	DNN based	✓		Image CS	✓	AMP algorithm
CSVideoNet [20]	DNN based			Video CS		RNN
SCSNet [30]	DNN based		✓	Image CS	✓	multi-rate CS
LAPRAN [34]	DNN based		✓	Image CS		multi-rate CS
OneNet [36]	Hybrid	✓	✓	Image CS		Plug-and-Play ADMM
CSDIP [37]	Hybrid		✓	Image CS		Deep-Image-Prior
CSMCNet	DNN based	✓		Video CS		motion estimation
CSMCNet-ITP	DNN based	✓	✓	Video CS		motion estimation/interpolation

TABLE III
THE COMPARISON RESULTS OF CSMCNet-3 WITH OTHER 7 METHODS ON VIDEO DATASET

Methods	$cr = 20\%$	$cr = 10\%$	$cr = 5\%$	$cr = 3\%$	$cr = 2\%$	speed(s)
CSVideoNet [20]	38.16/0.941	35.41 /0.903	32.01/0.865	30.13/0.823	28.62/0.789	10^{-1}
AMPNet [35]	37.44/0.952	32.99/0.908	29.04/0.847	27.3/0.813	25.67/0.781	10^{-1}
ReconNet [19]	37.12/0.904	32.11/0.878	28.63/0.752	26.62/0.631	25.49/0.617	10^{-1}
ISTANet [24]	37.93/ 0.955	31.64/0.877	29.02/0.840	27.31/0.793	25.7/0.761	10^{-2}
MC-BCS-SPL [15]	34.25/0.891	30.5/0.686	27.61/0.506	25.96/0.421	19.42/0.246	10^3
DAMP [32]	34.2/0.758	30.5/0.714	26.54/0.673	20.65/0.446	8.69/0.064	10^1
OneNet [36]	34.6/0.944	31.72/ 0.919	29.08/0.866	26.57/0.785	22.31/0.617	10^3
CSMCNet-3	38.34 /0.943	34.76/0.909	32.07/0.875	30.89/0.857	29.34/0.839	10^{-1}

ability of the MHME module. Therefore, the loss function for CSMCNet-K and CSMCNet-ITP-K is designed as follows

$$L(w, b) = L_{err} + \lambda L_{mc} \quad (15)$$

$$\begin{cases} L_{err} = \frac{1}{2N} \sum_i^T \|f(y_i; W, b) - x_i\|_2^2, \\ L_{mc} = \frac{1}{2N} \sum_i^T \|y_i - \Phi_B x_{mc}\|_2^2. \end{cases} \quad (16)$$

where λ is the scale factor to control the influence of motion compensation on the total loss. Determined by experiment, we set λ to be 0.5 during training.

We choose MSE to calculate loss and the proposed network can also be adapted to other loss functions. Adaptive moment estimation (Adam) optimizer with default parameters is used to optimize the network.

V. EXPERIMENTS

In this section, we firstly introduce the experimental settings in Sec.V-A, and compare our method with the-state-of-arts CS reconstruction methods in Sec.V-B, including conventional iterative methods and DNN based methods, both on image CS and video CS. Then in Sec.V-C, CSMCnet-K with $K = 1, 2, 3, 4, 5$ is tested to evaluate the influence of stage number. The generality of the ITP module is validated in Sec.V-D, and the performance of the ITP module is evaluated in Sec.V-E.

A. Experimental Settings

As there is no standard dataset for video CS, we use the vimeo-90K dataset [39] to build our own training dataset. vimeo-90K dataset contains 89800 high quality video clips from vimeo.com. We extract only the luminance component

of the video and crop the central 160×160 patch from each frame. We randomly choose videos from vimeo-90K dataset and get around 20,000 pairs of data for training and validation. To simulate the situation of inference, we produced reference frames of the training data pairs by using the output of image-specific CS reconstruction methods. A dataset containing 6 grey video sequences with the resolution of 1920×1280 is used to perform test on video CS reconstruction, and Set11 [28] is used to perform test on image CS reconstruction.

Our model is realized with PyTorch and all the experiments are performed on a workstation with an Intel Xeon CPU and a Nvidia GeForce RTX2080 GPU. In the experiments, we set the block size as 16×16 and choose $CR = 20\%, 10\%, 5\%, 3\%, 2\%$. We normalize the input pre-feature to zero mean and standard deviation one, and all trainable parameters of the network are initialized randomly with the default initialization function of PyTorch. All models are trained for 1,000,000 iterations with batch size 250 and learning rate 0.001. In the following sections, K is set to 3 for CSMCNet-K, since CSMCNet-3 achieves the best performance as evaluated in Sec.V-C.

The iterative methods used in the comparison are D-AMP [32] and MC-BCS-SPL [15]; The DNN based methods are ReconNet [19], ISTANet [24], AMPNet [35], CSVideoNet [20], SCSNet [30] and LAPRAN [34]; Hybrid methods OneNet [36] and CSDIP [37] are also included. Among these approaches, MC-BCS-SPL and CSVideoNet are specially designed for video CS tasks and others are for image CS tasks. ReconNet is a classical end-to-end deep network. ISTANet and AMPNet are deep unfolding methods, and the number of layers is set

TABLE IV
THE COMPARISON RESULTS OF CSMCNET-K WITH $K = 1, 2, 3, 4, 5$ ON VIDEO DATASET

Methods	$cr = 20\%$	$cr = 10\%$	$cr = 5\%$	$cr = 3\%$	$cr = 2\%$	Average
CSMCNet-1	37.84/0.938	34.44/0.899	31.87/0.857	29.52/0.823	28.22/0.799	32.37/0.863
CSMCNet-2	38.27/0.942	34.46/0.903	31.92/0.866	30.23/0.844	28.24/0.821	32.62/0.875
CSMCNet-3	38.34/0.943	34.76/0.909	32.07/0.875	30.89/0.857	29.34/0.839	33.08/0.885
CSMCNet-4	38.09/0.941	34.89/0.911	32.43/0.876	30.72/0.857	29.55/0.840	33.14/0.885
CSMCNet-5	38.22/0.943	35.01/0.910	32.49/0.874	30.65/0.853	29.19/0.839	33.11/0.883

to 6. SCSNet and LAPRAN are able to solve scalable CS reconstruction with one model. The summarized information about these algorithms is listed in Table II. Two metrics, peak signal-to-noise ratio (PSNR) and structural similarity (SSIM) are used to evaluate the performance quantitatively, and the flexibility of the methods is evaluated based on time consumption and parameter number. Besides, visualized results are also presented.

B. Comparison with State-of-the-arts

In this subsection, we compare our proposed CSMCNet-3 with other seven methods under different condition of compression ratio. The selected methods cover a variety of types, namely CSVideoNet [20], AMPNet [35], ReconNet [19], ISTANet [24], MC-BCS-SPL [15], DAMP [18] and OneNet [36], whose characteristic can be viewed in Table II. Before the experiments, we retrain the DNN based methods, namely CSVideoNet, AMPNet, ReconNet and ISTANet on the dataset described before and 6 video sequences with resolution of 1280x720 are used as test dataset. All the methods used in the experiments reconstruct images block-by-block and the denoising operation and sampling matrix optimization is forbidden for fairness.

The results of comparison are concluded in Table III. We test the methods at CS ratios of 20%, 10%, 5%, 3%, 2%. We calculate the corresponding PSNR and SSIM value as the indicator of reconstruction quality, and reconstruction speed is also considered. The best results are bolded. Since the time consumption can be affected by various factors, such as hardware performance, CPU workload, acceleration of GPU and compilation and execution speed of the programming language, we only show the order of magnitude of the speed in the table.

As shown in Table III, generally, DNN based methods have better reconstruction quality than optimization based methods, especially for low CR conditions, verifying the effectiveness of the parameters learned by convolution layers. Besides, the speed of DNN based methods is several orders of magnitude faster than iterative methods due to their feed-forward architecture and the acceleration of GPU. Another noteworthy point is that benefited from the utilization of inter-frame information, CSMCNet-3 and CSVideoNet can further improve the recovery quality compared with other image specific DNN methods, and the performance improvement is larger at lower CS ratio. Moreover, compared with the RNN module used in CSVideoNet, the explicit MH motion estimation module employed in our model provides better reconstruction results. The reason may be that the RNN module is not purposefully

optimized, and the interpretable structure has a more explicit improvement objective.

Visual results of the reconstruction of different methods are shown in Fig.10, and PSNR and SSIM value is indicated below the images. The results are obtained under condition of $CR = 10\%$, and no post denoiser is used. As presented in the visual results, the proposed CSMCNet suffers less block effect compared with other block-based CS methods, demonstrating better uniformity of our approach. Besides, our method also produces relatively richer and more accurate details in the highlight areas, leading to better subjective image quality evaluation.

C. Evaluating Stages of CSMCNet-K

In this subsection, we evaluate the influence of the stage number. CSMCNet-K with $K = 1, 2, 3, 4, 5$ is tested on 6 video sequences at CS ratios of 20%, 10%, 5%, 3%, 2%. The results are shown in Table IV, and the best results are bolded.

As described earlier, the number of stages of CSMCNet-K corresponds to the number of iterations of the unfolded algorithm. From Table IV, it can be found that as the number of stages increases from 1 to 4, the performance improves. It is understandable that deeper network gains better learning capability. However, the performance deteriorates at CSMCNet-5, and we speculate that deeper structure makes the model more difficult to converge during training. Moreover, the time consumption and memory space required to train the network also increases with more stages. Therefore, to strike a balance between the quality of reconstruction and the cost of training, we empirically decide to use CSMCNet-3 to compare with other reference methods.

D. Validating the Universality of the ITP Module

In this subsection, we validate the generality of the ITP module. To prove that the ITP module can be easily applied to different deep learning models, we plug the ITP module into several methods, including CSMCNet-3, CSVideoNet [20], ReconNet [19], ISTANet [24] and AMPNet [35]. We compare their performance with the original models on both video sequences and image dataset at CS ratios of 20%, 10%, 5%, 3%, 2%. The video sequences are the same as used in Sec.V-B, and the image dataset is Set11 [28]. No denoising strategy and sampling matrix optimization is used. All models without ITP module are trained separately at different CS ratios and those having ITP module are only trained once.

Fig.8 shows the comparison results. It can be found that compared with the original methods, the plugged-in methods

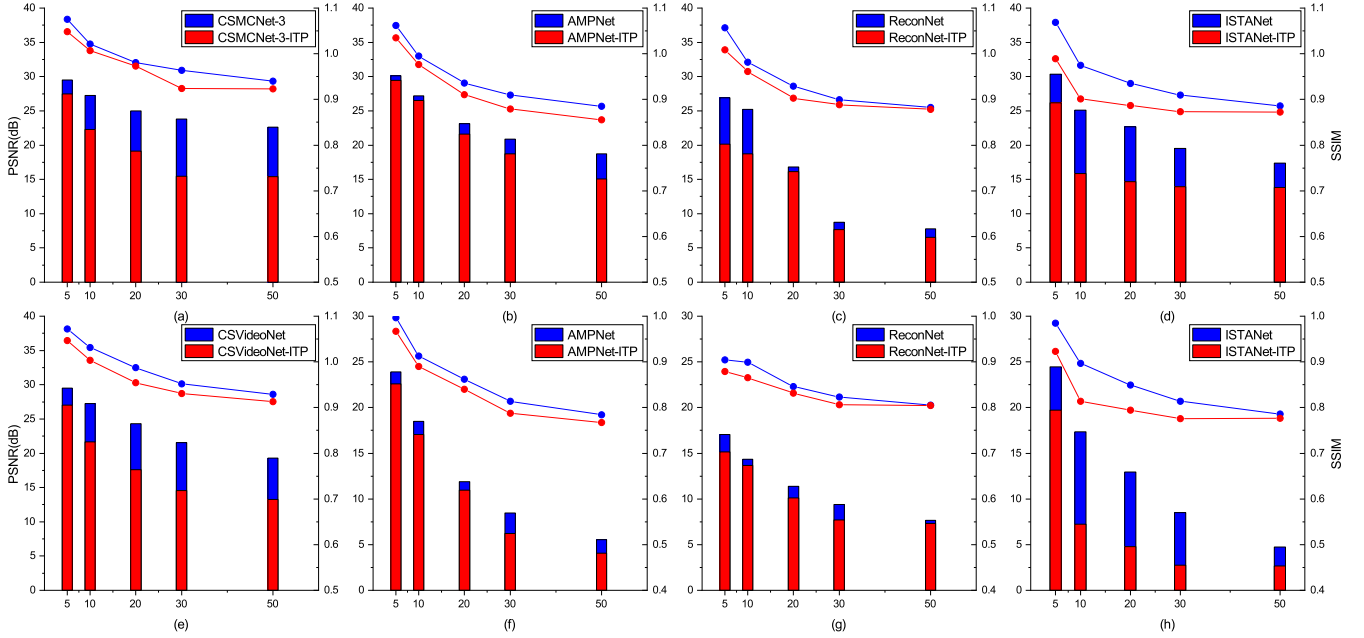


Fig. 8. The results of comparison between ITP methods and original models. Sub-figures (a)-(e) are tested on video dataset and sub-figures (f)-(h) are tested on Set11. The ITP-plugged-in methods are marked in red and the original methods are marked in blue. For each sub-figure, the line+symbol graph shows the PSNR value and the bar graph shows the SSIM value.

TABLE V
THE COMPARISON RESULTS OF THREE ITP METHODS WITH 5 OTHER SCALABLE CS METHODS ON SET11

Methods	$cr = 20\%$	$cr = 10\%$	$cr = 5\%$	$cr = 3\%$	speed	model size
AMPNet-ITP	28.36/0.852	24.48/0.741	22.01/0.619	19.36/0.524	10^{-1}	3.2M
ReconNet-ITP	23.93/0.703	23.26/0.673	21.56/0.602	20.33/0.554	10^{-1}	0.1M
ISTANet-ITP	26.14/0.794	20.7/0.545	19.72/0.496	18.8/0.455	10^{-2}	0.5M
LAPRAN [34]	27.46/0.89	23.55/0.827	22.11/0.709	21.35/0.76	10^{-1}	279.9M
SCSNet [30]	31.82/0.921	28.52/0.862	25.85/0.784	--	10^{-1}	4.6M
CSDIP [37]	23.44/0.524	19.53/0.391	17.05/0.33	15.17/0.166	10^2	--
OneNet [36]	26.73/0.831	25.43/0.811	22.88/0.739	20.69/0.638	10^3	--
D-AMP [32]	24.48/0.733	19.56/0.422	12.85/0.098	8.8/0.09	10^1	--

have relatively worse performance, and the gap is larger at higher CS ratio. The reason may be that the ITP module cannot fully rebuild the distribution of the signal via interpolation, and as the number of interpolated elements increases at low CS ratio, the gap between them and the original distribution narrows down. This phenomenon proves the validity of the interpolation strategy.

Though the loss of reconstruction performance is to be expected, taking consideration of the parameter size of the models and the cost of training, the loss of performance is acceptable. As the ITP module is light weighted compared to the main body of reconstruction models, we can suppose that the parameter size and time consumption of training decreases by a factor of N under the same operating conditions, where the factor N is the number of CS ratios we want to apply. In our experiments, the ITP method saves 5 times the storage space and training time approximately, at the cost of a 10.92% drop in PSNR performance and a 8.27% drop in SSIM performance in average. Overall, we think this is an acceptable price to pay.

Besides, Fig.8 also shows that for some methods, such as AMPNet, ITP module is more effective, and for others, such as ISTANet, the strategy performs poorly. Our future research will focus on which types of methods will work better with the interpolation strategy.

E. Evaluating the ITP Module

In this subsection, we further compare the ITP methods with other scalable compression ratio methods, namely D-AMP [32], LAPRAN [34], SCSNet [30], OneNet [36] and CSDIP [37]. The first of them is an optimization based iterative method, the second and the third are scalable deep learning models with fixed network architecture, and the last two combines deep learning models with iterative steps. The detailed characteristic of these methods can be found in Table II. The test dataset is Set11 [28], and the test condition is $CSratio = 20\%, 10\%, 5\%, 3\%$. No sampling matrix optimization and deblocking strategy is used. In addition to PSNR and SSIM, which server as the objective image quality indicators, we also list the order of magnitude of speed for

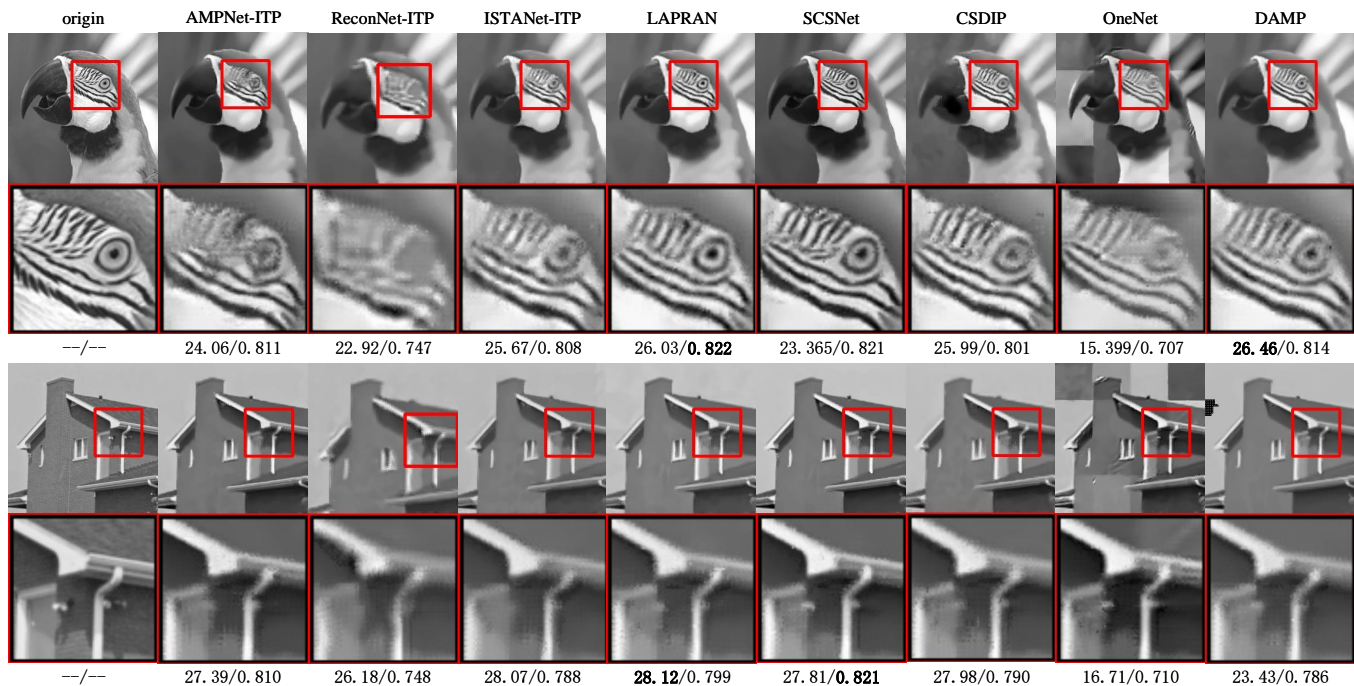


Fig. 9. The visualized output of 8 adaptive CS methods on *Parrots* image and *house* image at CS ratios of 20%. The output is denoised by BM3D to alleviate block effect. PSNR and SSIM value are indicated below the figures and the best results are bolded.

all methods and the model size for DNN based methods, which can be used as a metric to determine the ease of model deployment. The visualized results can be found in Fig.9.

As concluded in Table V, the ITP methods are at the forefront among all selected methods under different CR conditions, and the model size is well controlled. For D-AMP, its performance is good at high CR, but declines rapidly at low CR. The SCSNet has the best reconstruction quality, but its adaptive capability is achieved by combining sub-models dealing with different compression rates into one large model, leading to larger parameter size compared with ITP methods. The LAPRAN also achieves good performance, but the output of LAPRAN is of different size decided by the factor of compression ratio. The PSNR and SSIM results are calculated by interpolating the output of LAPRAN with bicubic algorithm, and this property is inconvenient for practical application. For OneNet and CSDIP, the disadvantage is that they are time-consuming. Besides, the visualized results of OneNet suffers severe blocking effect. We also want to point out that, as mentioned before, the performance of ITP-plugged-in methods is highly correlated with the original methods, and that is why AMPNet-ITP and ISTANet-ITP get relatively better results compared with ReconNet-ITP.

VI. CONCLUSION

In this paper, we design a deep neural network named CSMCNet based on the deep unfolding technique. The network performs video CS reconstruction and improves reconstruction quality with motion estimation. Experimental results prove the effectiveness of the proposed multi-hypothesis motion estimation module in utilizing temporal information of adjacent

frames in video sequences. Moreover, an interpolation module and corresponding training strategy is designed to implement scalable sampling and reconstruction, which is useful for flexible deployment. Finally, comprehensive comparison is conducted between proposed CSMCNet-3 and state-of-the-art reconstruction methods. CSMCNet-3 outperforms the reference methods in terms of reconstruction quality and speed. Additional experiments also demonstrate the ITP module's versatility. One potential direction of our future work is to find more suitable interpolation algorithm for the ITP module, and another direction is to evaluate the relationship of the ITP module and the following reconstruction networks.

REFERENCES

- [1] E. J. Candes and T. Tao, "Near-optimal signal recovery from random projections: Universal encoding strategies?" *IEEE Transactions on Information Theory*, vol. 52, no. 12, pp. 5406–5425, 2006.
- [2] M. F. Duarte, M. A. Davenport, D. Takhar, J. N. Laska, T. Sun, K. F. Kelly, and R. G. Baraniuk, "Single-pixel imaging via compressive sampling," *IEEE Signal Processing Magazine*, vol. 25, no. 2, pp. 83–91, 2008.
- [3] Y. Yang, J. Sun, H. Li, and Z. Xu, "Admm-csnet: A deep learning approach for image compressive sensing," *IEEE Transactions on Pattern Analysis and Machine Intelligence*, vol. 42, no. 3, pp. 521–538, 2020.
- [4] M. Iliadis, L. Spinoulas, and A. K. Katsaggelos, "Deep fully-connected networks for video compressive sensing," *Digital Signal Processing*, vol. 72, pp. 9–18, 2018.
- [5] R. G. Baraniuk, V. Cevher, M. F. Duarte, and C. Hegde, "Model-based compressive sensing," *IEEE Transactions on Information Theory*, vol. 56, no. 4, pp. 1982–2001, 2010.
- [6] M. Stéphane, *CHAPTER 1 - Sparse Representations*. Boston: Academic Press, 2009, pp. 1–31. [Online]. Available: <https://www.sciencedirect.com/science/article/pii/B9780123743701000057>
- [7] M. Elad. New York: Springer-Verlag New York, 2010.
- [8] E. J. Candès, J. K. Romberg, and T. Tao, "Stable signal recovery from incomplete and inaccurate measurements," *Communications on Pure and Applied Mathematics*, vol. 59, no. 8, pp. 1207–1223, 2006. [Online]. Available: <https://doi.org/10.1002/cpa.20124>

- [9] E. J. Candes and M. B. Wakin, "An introduction to compressive sampling," *IEEE Signal Processing Magazine*, vol. 25, no. 2, pp. 21–30, 2008.
- [10] R. Baraniuk, M. Davenport, R. DeVore, and M. Wakin, "A simple proof of the restricted isometry property for random matrices," *Constructive Approximation*, vol. 28, no. 3, pp. 253–263, 2008. [Online]. Available: <https://doi.org/10.1007/s00365-007-9003-x>
- [11] X. Yuan and R. Haimi-Cohen, "Image compression based on compressive sensing: End-to-end comparison with jpeg," *Ieee Transactions on Multimedia*, vol. 22, no. 11, pp. 2889–2904, 2020. [Online]. Available: [Go to ISI://WOS:000584239900010](https://www.ncbi.nlm.nih.gov/pubmed/25095253)
- [12] J. Zhou, J. Zhou, and L. Guo, "Angular intra prediction based measurement coding algorithm for compressively sensed image," in *international conference on multimedia and expo*, Conference Proceedings, pp. 1–6.
- [13] J. Zhou, D. Zhou, T. Yoshimura, and S. Goto, "Approximate-dct-derived measurement matrices with row-operation-based measurement compression and its vlsi architecture for compressed sensing," *IEICE Transactions on Electronics*, vol. E101.C, no. 4, pp. 263–272, 2018.
- [14] C. Li, W. Yin, H. Jiang, and Y. Zhang, "An efficient augmented lagrangian method with applications to total variation minimization," *Computational Optimization and Applications*, vol. 56, no. 3, pp. 507–530, 2013. [Online]. Available: <https://doi.org/10.1007/s10589-013-9576-1>
- [15] E. F. James, M. Sungkwang, and W. T. Eric, *Block-Based Compressed Sensing of Images and Video*, ser. Block-Based Compressed Sensing of Images and Video. now, 2012. [Online]. Available: <http://ieeexplore.ieee.org/document/8187406>
- [16] I. Daubechies, M. Defrise, and C. De Mol, "An iterative thresholding algorithm for linear inverse problems with a sparsity constraint," *Communications on Pure and Applied Mathematics*, vol. 57, no. 11, pp. 1413–1457, 2004. [Online]. Available: <https://onlinelibrary.wiley.com/doi/abs/10.1002/cpa.20042>
- [17] L. He and L. Carin, "Exploiting structure in wavelet-based bayesian compressive sensing," *IEEE Transactions on Signal Processing*, vol. 57, no. 9, pp. 3488–3497, 2009.
- [18] C. A. Metzler, A. Maleki, and R. G. Baraniuk, "Bm3d-amp: A new image recovery algorithm based on bm3d denoising," in *2015 IEEE International Conference on Image Processing (ICIP)*, Conference Proceedings, pp. 3116–3120.
- [19] K. Kulkarni, S. Lohit, P. Turaga, R. Kerviche, and A. Ashok, "Reconnet: Non-iterative reconstruction of images from compressively sensed measurements," in *2016 IEEE Conference on Computer Vision and Pattern Recognition (CVPR)*, Conference Proceedings, pp. 449–458.
- [20] K. Xu and F. Ren, "Csvideonet: A real-time end-to-end learning framework for high-frame-rate video compressive sensing," 03/2018 2018.
- [21] H. Yao, F. Dai, S. Zhang, Y. Zhang, Q. Tian, and C. Xu, "Dr2-net: Deep residual reconstruction network for image compressive sensing," *Neurocomputing*, vol. 359, pp. 483–493, 2019.
- [22] Y. Wu, M. Rosca, and T. Lillicrap, "Deep compressed sensing," in *ICML*, Conference Proceedings.
- [23] K. Gregor and Y. Lecun, "Learning fast approximations of sparse coding," in *international conference on machine learning*, Conference Proceedings, pp. 399–406.
- [24] J. Zhang and B. Ghanem, "Ista-net: Interpretable optimization-inspired deep network for image compressive sensing," in *Proceedings of the IEEE conference on computer vision and pattern recognition*, Conference Proceedings, pp. 1828–1837.
- [25] B. Huang, J. Zhou, X. Yan, M. Jing, R. Wan, and Y. Fan, "Cs-mcnet: a video compressive sensing reconstruction network with interpretable motion compensation," in *Proceedings of the Asian Conference on Computer Vision (ACCV)*, November 2020.
- [26] G. Lu, "Block compressed sensing of natural images," in *2007 15th International Conference on Digital Signal Processing*, Conference Proceedings, pp. 403–406.
- [27] A. Mousavi, A. B. Patel, and R. G. Baraniuk, "A deep learning approach to structured signal recovery," in *2015 53rd Annual Allerton Conference on Communication, Control, and Computing (Allerton)*, Conference Proceedings, pp. 1336–1343.
- [28] S. Lohit, K. Kulkarni, R. Kerviche, P. Turaga, and A. Ashok, "Convolutional neural networks for noniterative reconstruction of compressively sensed images," *IEEE Transactions on Computational Imaging*, vol. 4, no. 3, pp. 326–340, 2018.
- [29] W. Shi, F. Jiang, S. Liu, and D. Zhao, "Image compressed sensing using convolutional neural network," *IEEE Transactions on Image Processing*, vol. 29, pp. 375–388, 2020.
- [30] —, "Scalable convolutional neural network for image compressed sensing," in *Proceedings of the IEEE Conference on Computer Vision and Pattern Recognition*, Conference Proceedings, pp. 12 290–12 299.
- [31] D. Bhatnagar and S. Budhiraja, "Image compression using dct based compressive sensing and vector quantization," *International Journal of Computer Applications*, vol. 50, pp. 34–38, 2012.
- [32] C. A. Metzler, A. Maleki, and R. G. Baraniuk, "From denoising to compressed sensing," *IEEE Transactions on Information Theory*, vol. 62, no. 9, pp. 5117–5144, 2016.
- [33] J. Yang, X. Yuan, X. Liao, P. Llull, D. J. Brady, G. Sapiro, and L. Carin, "Video compressive sensing using gaussian mixture models," *IEEE Trans Image Process*, vol. 23, no. 11, pp. 4863–78, 2014. [Online]. Available: <https://www.ncbi.nlm.nih.gov/pubmed/25095253>
- [34] K. Xu, Z. Zhang, and F. Ren, "Lapran: A scalable laplacian pyramid reconstructive adversarial network for flexible compressive sensing reconstruction," in *The 15th European Conference on Computer Vision (ECCV'18)*, Conference Proceedings, pp. 491–507.
- [35] Z. Zhang, Y. Liu, J. Liu, F. Wen, and C. Zhu, "Amp-net: Denoising-based deep unfolding for compressive image sensing," *IEEE Transactions on Image Processing*, vol. 30, pp. 1487–1500, 2021.
- [36] J. H. R. Chang, C. Li, B. Póczos, B. V. K. V. Kumar, and A. C. Sankaranarayanan, "One network to solve them all — solving linear inverse problems using deep projection models," in *2017 IEEE International Conference on Computer Vision (ICCV)*, Conference Proceedings, pp. 5889–5898.
- [37] D. V. Veen, A. Jalal, E. Price, S. Vishwanath, and A. Dimakis, "Compressed sensing with deep image prior and learned regularization," *ArXiv*, vol. abs/1806.06438, 2018.
- [38] K. He, X. Zhang, S. Ren, and J. Sun, "Deep residual learning for image recognition," in *2016 IEEE Conference on Computer Vision and Pattern Recognition (CVPR)*, Conference Proceedings, pp. 770–778.
- [39] T. Xue, B. Chen, J. Wu, D. Wei, and W. T. Freeman, "Video enhancement with task-oriented flow," *International Journal of Computer Vision (IJCV)*, vol. 127, no. 8, pp. 1106–1125, 2019.

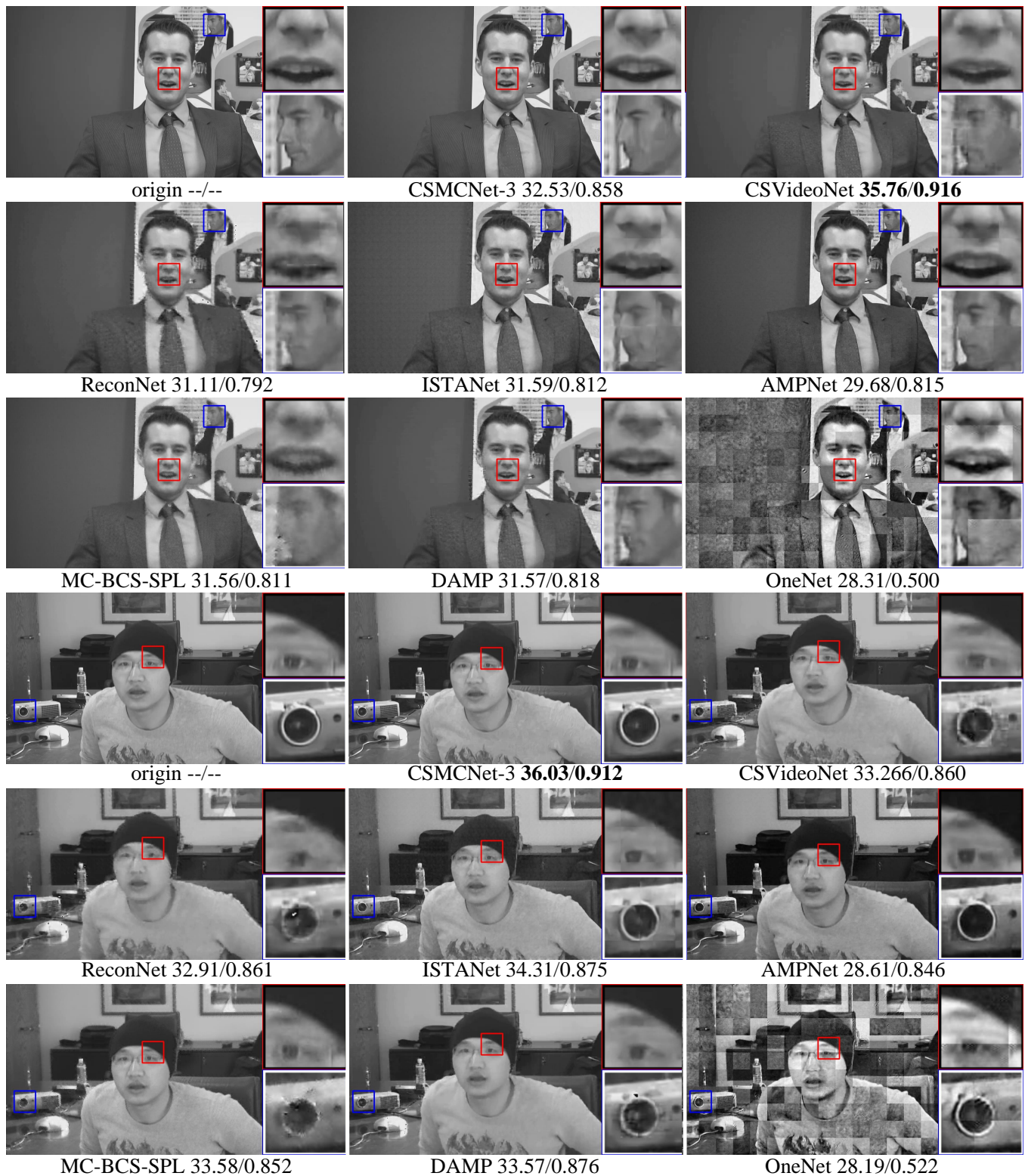


Fig. 10. The visualized output of CSMCNet-3, CSVideoNet [20], AMPNet [35], ReconNet [19], ISTANet [24], MC-BCS-SPL [15], DAMP [32] and OneNet [36] on one frame of *Johnny* and *vidyo4* at CS ratio of 10%. No deblocking methods are used. PSNR/SSIM value is indicated below the figures and the best results are bolded.